Post-translational control is sufficient to coordinate membrane synthesis with growth in *Escherichia coli*

Running title: Economy of membrane synthesis in E. coli

Marek J Noga[†], Ferhat Büke, Niels JF van den Broek[‡], Nicole Imholz, Nicole Scherer, Gregory Bokinsky*

Department of Bionanoscience, Kavli Institute of Nanoscience, Delft University of Technology, Delft, The Netherlands

Materials and correspondence: *e-mail: g.e.bokinsky@tudelft.nl

[†] Current address: Translational Metabolic Laboratory, Department of Laboratory Medicine, Radboud UMC, Nijmegen, The Netherlands

[‡] Current address: Vaccine Process & Analytical Development, Janssen Vaccines & Prevention B.V., Leiden, The Netherlands

Abstract

Every cell must produce enough membrane to contain itself. However, the mechanisms by which cells couple the rate of membrane synthesis with the rate of growth remain unresolved. By measuring precursors, intermediates, and enzymes of the fatty acid and phospholipid synthesis pathways of *Escherichia coli*, we show that while fatty acid and membrane synthesis capacities are maintained at a constant level across a 3-fold range of growth rates, the steady-state rate of phospholipid synthesis is principally mediated by allosteric control of a single enzyme, PlsB. Surprisingly, metabolic modelling indicates that PlsB activity also strongly influences flux into the synthesis pathway of lipopolysaccharide, the second-most abundant membrane component. In contrast to steady-state regulation, we find that responses to environmental perturbations are triggered directly via changes in acetyl-CoA concentrations, enabling rapid adaptation. Adaptations are further modulated by ppGpp, which regulates PlsB activity during slow growth and growth arrest. The strong reliance upon post-translational regulation for flux control ensures both robustness and responsiveness of membrane synthesis.

Introduction

The viability of growing cells demands that membrane synthesis be tightly orchestrated with biomass production. The asymmetric architecture and composition of the cell envelope in Gram-negative bacteria demands further coordination between multiple pathways that synthesize membrane components: phospholipid (PL) synthesis must be balanced with lipopolysaccharide (LPS) synthesis to ensure membrane stability (1, 2). PL and LPS pathways must also be coordinated with protein synthesis, which supplies the lipoproteins that tether the outer membrane to peptidoglycan (3). Although several targets and mechanisms of regulation have been identified or proposed in the model organism *Escherichia coli*, how cells use these regulation points to control membrane synthesis remains unclear (4).

Reaction rates (metabolic fluxes) may be modulated through either transcriptional regulation, which adjusts enzyme concentrations, or by post-translational mechanisms that adjust the activities of enzymes that are already present. For instance, the steady-state synthesis rate of proteins is widely thought to be controlled in many bacteria by ribosome abundance, which is transcriptionally regulated to balance amino acid supply with consumption (5). In contrast, fluxes through many essential metabolic pathways are determined instead by steady-state concentrations of substrates and inhibitors (post-translational regulation) rather than by transcriptional regulation (6, 7). Although post-translational regulation has long been known to play a significant role in membrane synthesis (8, 9) (10–12), the exact contributions of transcriptional and post-translational control to the coordination of membrane synthesis with growth remain unclear.

In order to understand how the membrane synthesis rate is coordinated with the growth rate (μ), we quantified enzymes, substrates and intermediates of the fatty acid and PL synthesis pathways in steady-state and dynamic conditions. We find that allosteric regulation of the first enzyme in the PL synthesis pathway, PlsB, ensures μ-dependent regulation of PL synthesis and

strongly influences flux into the LPS synthesis pathway. We furthermore find that the fatty acid and PL synthesis pathways are highly sensitive to changes in precursor concentrations caused by internal and external metabolic shifts. This sensitivity enables a rapid response to environmental changes that can be further modulated by allosteric inhibitors such as the global regulator guanosine tetraphosphate (ppGpp).

Results

The PL to biomass ratio varies inversely with μ

Lipid precursors of both LPS and PL are synthesized in the cytosol as fatty acyl thioesters covalently attached to the acyl carrier protein (acyl-ACP). PL are synthesized by membrane-bound enzymes from long-chain acyl-ACP and *sn*-glycerol-3 phosphate (G3P). G3P is produced either from glyceraldehyde-3-phosphate, an intermediate of central carbon metabolism, or via glycerol catabolism **(Figure 1A)**. We grew cultures of *E. coli* NCM3722 in 6 defined media that support a 3-fold range of μ (MOPS medium containing 0.2% acetate, succinate, malate, glycerol, glucose, or glucose with Cas-amino acids). Quantities of phosphatidylglycerol (PG), phosphatidylethanolamine (PE), and cardiolipin (CL) per unit biomass (as determined by culture optical density (OD) (13)) decreased with increasing μ **(Figure 1B)**, consistent with previous observations in *E. coli* and other bacteria (14, 15). The PG/PE ratio remained constant across all μ. We quantified steady-state PL flux by multiplying total PE LC/MS counts by μ, which closely approximates the overall PL synthesis rate as PE turnover is slow relative to synthesis (16). PL flux decreased by 2-fold over 3-fold range of μ **(Figure 1C)**. The higher PL to biomass ratio of slow-growing cells likely reflects their higher surface-to-volume ratio (17).

Allosteric regulation of PlsB activity is sufficient to couple PL flux with μ

We first sought to evaluate whether steady-state substrate concentrations determine PL flux. If the PL and fatty acid synthesis rates are modulated by substrate concentrations during steady-state growth, concentrations of these species would necessarily correlate positively with μ and PL flux. We quantified nucleotides, G3P, acyl-ACP, and PL synthesis intermediates using LC/MS (18). No correlation was observed between concentrations of the fatty acid precursor acetyl-CoA or with μ (**Figure 1D**). We also found no significant correlation between PL flux and

long-chain acyl-ACP substrates of PL synthesis **(Figure 1E,** Pearson correlation coefficients $r < 0.4$, $p > 0.4$, **Supplemental Table 1).** Although G3P concentrations correlate strongly with PL flux ($r > 0.99$), growth in glycerol medium increased G3P by 20-fold without affecting PL content or flux. These trends imply that steady-state PL flux is not modulated by fatty acid or PL precursor concentrations.

In contrast to PL synthesis substrates, concentrations of the fatty acid initiation and elongation substrate malonyl-ACP strongly correlate with PL flux **(Figure 1E,** $r = 0.9$, **Supplemental Table 1)**, suggesting that the fatty acid initiation and elongation rates are determined by malonyl-ACP concentrations and thus by the rate of malonyl-ACP synthesis by ACC and FabD. Concentrations of hydroxyl-acyl-ACP intermediates, including C14:0-OH-ACP, the lipid precursor of LPS, also correlate strongly with PL flux ($r > 0.99$), implying a simple flux-sensitive coupling mechanism between the PL and LPS synthesis pathways **(Figure 1E, Supplemental Figure 1)**. As ACC substrates acetyl-CoA and ATP do not correlate with μ **(Figure 1D, Supplemental Figure 2)**, and as concentrations of ACC protein subunits and FabD also do not correlate significantly with PL flux (**Supplemental Figure 3, Supplemental Table 1**), we infer that ACC activity is primarily modulated during steady-state conditions via allosteric control. Biochemical experiments have identified several regulators of ACC activity, including nitrogen-responsive regulator GlnB (19) and acyl-ACP substrates of PL synthesis (20).

Unlike long-chain acyl-ACP, the concentrations of all PL synthesis intermediates downstream of PlsB correlate tightly with PL flux **(Figure 1F,** $r > 0.89$-0.99, **Supplemental Table 1**). The contrast between the trends observed in substrates and products of PlsB suggests that the rates of the reactions following PlsB are primarily determined by substrate concentrations, further implying that transcriptional regulation of PlsB concentration or post-translational regulation of PlsB activity is sufficient to regulate flux into the PL pathway. Transcription of *plsB,* and thus PlsB abundance, is controlled by the μ-sensitive regulator guanosine tetraphosphate

(ppGpp) (21) and by the membrane stress-activated sigma factor RpoE (22). Concentrations of ppGpp are inversely correlated with μ **(Figure 1D)**, implying that PL flux may be coupled to μ by transcriptional control of the *plsB* gene by ppGpp. We measured fatty acid and PL synthesis pathway enzymes in each culture using LC/MS to determine whether enzyme concentrations are adjusted to couple PL flux with μ. We found no significant correlation between PL synthesis flux and PlsB concentration (**Figure 1G, Supplemental Table 1,** p >0.1). Instead, PlsB concentrations per unit biomass (OD) are nearly constant across the conditions studied, indicating that PlsB can accommodate at least a 2-fold range of PL flux without a corresponding change in concentration. Surprisingly, the concentrations of most fatty acid synthesis pathway enzymes also do not correlate significantly with PL flux **(Supplemental Table 1, Supplemental Figure 3).** The lack of correlation between PL flux and concentrations of PlsB or its acyl-ACP substrates implies that PL flux is regulated via allosteric control of PlsB.

μ can also be modulated independently of culture conditions by artificially varying ppGpp **(Figure 1D).** Titrating ppGpp above basal concentrations, but far below concentrations experienced during starvation, reduces steady-state μ by reducing ribosomal RNA synthesis (23). Furthermore, PlsB activity is inhibited at high ppGpp concentrations encountered during starvation (24). We titrated μ by expressing the catalytic domain of the ppGpp synthesis enzyme RelA (RelA*) from an inducible promoter (P_{Tet}) in glucose medium. As previously observed (23), RelA*-titrated cultures exhibit ppGpp concentrations that are elevated 2-fold above wild-type cultures growing at similar rates **(Figure 1D).** Trends in PL abundance, PL flux, acyl-ACP species, PL intermediates, and PL synthesis enzyme concentrations in ppGpp-limited cultures are highly similar to trends observed as μ is varied by carbon source **(Figure 1B-C, 1E-G, Supplemental Figures 1, 3).** Concentrations of PlsB and fatty acid pathway enzymes do not substantially vary in ppGpp-limited cultures **(Figure 1G, Supplemental Figure 3)**. The trends in substrate, enzyme, and intermediate concentrations observed in ppGpp-limited cultures are

consistent with regulation of PL flux occurring via allosteric control of PlsB. Unexpectedly, concentrations of LpxC, which catalyses the committed step in the LPS pathway (25), decrease 2-fold as PE flux increases **(Supplemental Figure 3).**

Mathematical modelling supports PlsB control of steady-state PL synthesis

To test whether modulation of PlsB activity alone is sufficient to govern PL synthesis flux, we constructed a simplified differential equation model of fatty acid, LPS initiation, and PL biosynthesis **(Figure 2A).** The model includes competitive inhibition of ACC by C16:0-ACP as the sole regulatory interaction. The model also includes a branch point at C14:0-OH-ACP into LPS synthesis. This branch point is represented by a single step that combines reactions catalysed by LpxA and LpxC, as LpxC catalyses the first irreversible reaction in the LPS pathway (25). Concentrations of G3P and C16:1-ACP are fixed in the model to reflect experimental observations of enzyme saturation and substrate invariance, respectively (see **Supplementary Methods** for model details, parameter sets, and sensitivity analysis).

We used the model to predict which enzymes and substrates exert control over PL and LPS flux. Increasing ACC and PlsB V_{max} parameters by 4-fold each increased PE and LPS synthesis fluxes in parallel by 2-fold, while changes in the V_{max} parameters of all other enzymes in the model had little or no effect on simulated PE flux. Surprisingly, simulated LPS flux correlates positively with PlsB activity when LpxC V_{max} is held constant due to the coupling between PE flux and concentrations of the LPS precursor, C14:0-OH-ACP. Changes in the C14:0-OH-ACP dehydration reduction rate and LPS initiation rate (catalysed in the model by FabZ and LpxC, respectively) exerted strong and opposite effects on LPS flux without significantly changing PE flux. Increasing the V_{max} parameters of PL synthesis enzymes downstream of PlsB also did not change PE synthesis flux, suggesting that the observed variations in PlsC and CdsA concentrations do not affect PE flux. Of the two substrates

considered (acetyl-CoA and C16:1-ACP), only variations in acetyl-CoA strongly influences PL and LPS flux **(Figure 2B)**.

Simulated variations in acetyl-CoA concentrations and ACC and PlsB enzyme V_{max} parameters generate changes in intermediate concentrations that closely reproduce most experimentally-observed trends, supporting our model. However, our steady-state measurements strongly contradict simulated C16:0-ACP concentration trends caused by variations in acetyl-CoA and ACC activity. Simulated variations in PlsB V_{max} closely approximate observed C16:0-ACP trends (**Figure 2C).** We therefore conclude that PL synthesis flux is primarily regulated during steady-state growth by allosteric control of PlsB activity. However, changes in acetyl-CoA concentration or ACC activity may also influence PL flux during environmental or metabolic perturbations.

Translation inhibition causes carbon overflow into fatty acid synthesis

We set out to evaluate whether a known allosteric regulator of PlsB, ppGpp, is able to directly regulate PlsB activity during steady-state growth. High concentrations of ppGpp are known to inhibit PlsB (24), while low concentrations of ppGpp correlate inversely with μ **(Figure 1D).** The notion that ppGpp concentrations might regulate PL synthesis even at the low basal concentrations present during steady-state growth has been proposed but never tested (26). Although steady-state PlsB activity clearly decreased in response to ppGpp titration, the mode of control by ppGpp (transcriptional regulation of a PlsB-regulating process or protein, or direct post-translational inhibition) cannot be determined from steady-state data alone. We first wished to observe the effects of high concentrations of ppGpp on fatty acid and PL synthesis using our assay. Synthesis of high concentrations of ppGpp by RelA (the stringent response) is triggered by any stress or starvation conditions that lead to the specific biochemical cue of uncharged tRNA bound to the ribosome. During the stringent response, ppGpp accumulates by more than

10-fold over basal concentrations and PL synthesis rates are reduced by approximately half (24, 26), likely due to PlsB inhibition (27).

We triggered ppGpp accumulation by adding the tRNA aminoacylation inhibitor mupirocin to glucose cultures of wild-type and Δ*relA E. coli*. Mupirocin inhibits translation in both strains and causes a 10-fold accumulation of ppGpp in the wild-type strain within 1 minute to over 400 pmol/OD, reaching >800 pmol/OD after 3 minutes **(Supplemental Figures 4, 5).** To our surprise, mupirocin treatment also transiently increased malonyl-ACP and hydroxyl-ACP at the expense of holo-ACP in both strains **(Figure 3A, Supplemental Figure 6)**. The increase in acyl-ACP is matched by a corresponding increase in PL synthesis intermediates, suggesting that mupirocin diverts a pulse of carbon into the fatty acid pathway that is efficiently transmitted into PL synthesis **(Figure 3B)**. In the wild-type strain, the pulse of fatty acid synthesis activity is rapidly followed by C16:0- and C18:0-ACP accumulation, consistent with ppGpp inhibition of PlsB **(Figure 3A, Supplemental Figure 6)**. C16:0-ACP accumulation is followed in turn by an increase in holo-ACP and a decrease in malonyl-ACP, indicating ACC inhibition **(Figure 3A)**. PL intermediates PA, PS, and PGP are rapidly depleted in the wild-type strain after briefly increasing **(Figure 3B).** The transient carbon influx shifts acyl chains incorporated into PL towards longer-chain fatty acids, likely due to increased malonyl-ACP concentrations favouring fatty acid elongation at the expense of membrane incorporation by PlsB and PlsC **(Supplemental Figure 7).** While suppression of fatty acid synthesis in the wild-type strain can be attributed to ppGpp, it is unclear what attenuates the carbon influx in the Δ*relA* strain; however eventual C14:0-ACP accumulation likely contributes to ACC inhibition. Inhibition of fatty acid elongation also depletes LPS precursor C14:0-OH-ACP, which is expected to decrease LPS synthesis in parallel with PL synthesis **(Figure 3A)**.

As the transient increase in malonyl-ACP after mupirocin treatment occurs in both wild-type and Δ*relA* strains, we hypothesized that translation inhibition somehow channels excess

carbon into lipid synthesis. We added the ribosome inhibitor chloramphenicol and the transcription initiation inhibitor rifampicin to glycerol cultures of wild-type *E. coli*. Both compounds inhibit translation via mechanisms that suppress ppGpp synthesis. As with mupirocin, chloramphenicol triggered a rapid decrease in holo-ACP and an increase in long-chain unsaturated acyl-ACP species C16:1-ACP and C18:1-ACP **(Figure 3C).** Both antibiotics triggered an increase in PL synthesis intermediates PA and PS that resembled the increase observed in the Δ*relA* strain after mupirocin treatment **(Figure 3D).**

What might cause the transient increase in fatty acid synthesis observed after translation inhibition? Interestingly, both rifampicin and chloramphenicol increased acetyl-CoA concentrations by 3-fold **(Figure 3E)**, suggesting a possible cause. Acetyl-CoA also increased in both the wild-type and the Δ*relA* strain after mupirocin addition in glucose medium before decreasing ~30% in the wild-type strain **(Supplemental Figures 4, 5).** While it is unclear why translation inhibition would increase acetyl-CoA, the observed response of the fatty acid pathway is consistent with our mathematical model, which predicts fatty acid flux to be highly sensitive to acetyl-CoA. We confirmed the sensitivity of the fatty acid and PL synthesis pathways to environmental changes using a fast nutritional upshift. Addition of glucose and amino acids to a glycerol culture also caused a rapid accumulation of PA and PS species that resemble the increases observed following translation inhibition **(Supplemental Figure 8).**

Moderate ppGpp concentrations regulate PlsB via post-translational control

In order to clearly discern the effects of ppGpp on the fatty acid and PL synthesis pathways without complications introduced by translation inhibition, we monitored fatty acid and PL synthesis pathways after inducing RelA*. The response in the fatty acid and PL synthesis pathways is consistent with PlsB inhibition by ppGpp followed by ACC activity suppression by accumulated long-chain acyl-ACP, depleting malonyl-ACP **(Figure 4A)**. PL intermediates also respond in a manner consistent with PlsB inhibition: LPA species steadily decrease, followed by

PA, PS, and PG **(Figure 4B)**. Addition of chloramphenicol 10 minutes following RelA* induction causes an increase in unsaturated long-chain acyl-ACP, though the response of the PL pathway is attenuated. We note that the PS pool is depleted more after ppGpp induction than the LPA and PA pools, suggesting an additional regulatory mechanism downstream of PlsB.

We next sought to evaluate whether basal ppGpp concentrations are also capable of regulating PlsB via post-translational control. As the effects of post-translational control are more rapidly apparent than those that follow transcriptional regulation, we followed the timescale of the response of the PL pathway to ppGpp synthesis. We measured ppGpp and PL synthesis intermediates during RelA* induction to moderate levels. ppGpp increased within 10 minutes of RelA* induction and reached its elevated steady-state concentration (~150 pmol/OD) by 20 minutes. Concentrations of PL intermediates PA and PS began to decrease within 10 minutes **(Figure 4C)**. Interestingly, PS decreases further after ~25 minutes, at which point PA increases slightly, suggesting that PS may be back-converted to PA by PssA (28) **(Figure 4C).** The immediate decay of PA and PS pools indicates that ppGpp inhibits PlsB via post-translational regulation at moderate concentrations. To verify that the immediate PA and PS depletion is too fast to be explained by transcriptional regulation, we compared the PA and PS response kinetics with the kinetics of a ppGpp-driven response known to be mediated by transcriptional control. Cyclopropyl PL are produced from unsaturated fatty acids of membrane PL by the enzyme Cfa, expression of which is induced transcriptionally by ppGpp (29). PL cyclopropylation begins 25 minutes after RelA* induction, much slower than the decrease in PA and PS. We conclude that the rapid decrease in PA and PS 5-10 minutes after RelA* induction is mediated via post-translational regulation of PlsB.

We used our model to simulate the observed response of PA and PS concentrations immediately following mild RelA induction (up to 25 minutes post-induction) in order to estimate the concentrations at which ppGpp inhibits PlsB. As the mode of inhibition is unknown (i.e.

competitive inhibition, mixed inhibition, or indirect inhibition via a ppGpp-responsive mediator), we used an empirical allosteric inhibition term to obtain an effective K_I parameter (model details provided in **Supplemental Methods)**. We estimate K_I to be approximately 300 pmol/OD, well above the concentrations observed during the slowest steady-state growth condition used here (60 pmol/OD at μ ~ 0.5 /hr). Direct ppGpp inhibition of PlsB may be relevant to PL flux during extremely slow growth when ppGpp concentrations are above 150 pmol/OD, which may occur at μ well below 0.5 hr^{-1}.

Discussion

Our comprehensive characterization and modelling of the fatty acid and PL biosynthesis pathways establishes the specific regulatory tools used by *E. coli* to couple membrane synthesis with μ. Most importantly, we find that allosteric control of PlsB is sufficient to balance steady-state PL flux with μ. PlsB demand controls flux into the fatty acid pathway through ACC via inhibition by PlsB substrates, consistent with metabolic control theory (30). Membrane synthesis is regulated very differently than protein synthesis, as membrane synthesis capacity (i.e. concentrations of PlsB and fatty acid synthesis pathway enzymes) is maintained at stable levels across a 3-fold range of μ. Counterintuitively, increased transcription of the fatty acid and PL synthesis pathways reported to occur at higher μ (31) does not increase concentrations of these enzymes, but rather maintains them at a constant concentration. Maintaining a constant capacity for membrane synthesis enables the cell to address any change in membrane synthesis demand at the cost of expressing enzymes that remain inhibited at slow or moderate μ (32).

Both our model and our experimental data indicate that ACC and PlsB activities determine the concentrations of LPS precursor C14:0-OH-ACP, indicating that PL synthesis control also plays a role in coordinating LPS synthesis flux with μ. Perhaps counterintuitively, increasing PL synthesis does not come at the cost of LPS flux, but rather, increases in PL flux directly increase C14:0-OH-ACP by relieving feedback inhibition of ACC. As we observed that LpxC concentrations decrease in response to higher μ, we propose that LpxC concentrations are regulated in response to over-accumulation of LPS that occurs due to increasing concentrations of C14:0-OH-ACP. This regulation may be mediated by increased degradation by the FtsH protease (33), although we cannot exclude that LpxC concentrations are also modulated by transcriptional regulation. Our data will be essential in evaluating existing models of PL-LPS pathway coordination (34).

Although PlsB determines PL flux during steady-state growth, this control is not absolute, as the fatty acid and PL pathways (and likely the LPS pathway) are highly sensitive to fluctuations in acetyl-CoA concentrations and ACC activity. The sensitivity of PL flux to central metabolism and even protein synthesis arrest renders membrane synthesis extremely responsive to small environmental changes. While this sensitivity facilitates rapid adaptation of PL flux to changes in μ, the tight connection between protein synthesis, central carbon metabolism, and membrane biogenesis demands additional allosteric control (including inhibition by ppGpp) to re-balance the pathway with μ and prevent PL overflow. If protein synthesis is inhibited in a manner that does not decrease carbon flow into the fatty acid pathway (e.g. by sudden nitrogen starvation), we hypothesize that continued PL and LPS synthesis would outpace synthesis of the lipoproteins that tether the outer membrane to the peptidoglycan layer. Inhibition of PL and LPS pathways by ppGpp would thus prevent production of excess membrane, enforcing the coupling of PL and lipoprotein synthesis. Consistent with this notion, strains lacking the ppGpp response (known as relaxed strains) have been observed to generate higher quantities of extracellular PL and LPS, likely as outer membrane vesicles (35).

We estimate that post-translational control of PlsB by ppGpp, reflected by a relatively high effective K_I (~300 pmol/OD), suggests that ppGpp contributes to steady-state membrane synthesis regulation during growth in conditions that support $\mu > 0.5\ hr^{-1}$. Although it is generally believed that ppGpp directly inhibits PlsB, multiple groups have been unable to observe ppGpp inhibition of PlsB *in vitro* when acyl-ACP are used as substrates (36, 37). ppGpp may therefore control PlsB indirectly by modulating activity of a regulator or a cellular process that interacts with PlsB. Several candidates for the allosteric regulator of PlsB activity have been discovered. In immunoprecipitation experiments, PlsB has been found to interact with proteins including ACP and PssA, as well as several whose roles are unclear (PlsX and YbgC) (38), suggesting that PlsB forms part of a PL synthesis complex that may couple PlsB activity with μ. As PL synthesis

flux has been observed to oscillate with the cell division cycle in *E. coli* and other bacteria (39), PlsB may also be regulated by the divisome or by septum formation. Degradation of PL by phospholipases may also play an important role in membrane homeostasis during steady-state growth (40), as is known to occur during growth and division in eukaryotes (41). In addition to identifying the allosteric regulators of PlsB, studies that integrate connections between PL catabolism and transport with PL synthesis are needed for a comprehensive understanding of membrane homeostasis.

Acknowledgements

We thank Michael Cashel for providing *E. coli* strain CF7974. We thank Christophe Danelon, Bertus Beaumont, and Frank Bruggeman for invaluable suggestions for improving the manuscript. This research was funded by a grant to GB from the Netherlands Organisation for Scientific Research (ALW Open 824.15.018) and an award from the Frontiers of Nanoscience program.

Conflict of Interest

The authors declare that they have no conflict of interest.

Author contributions

MN and GB designed the experiments. MN, FB, NvdB, NS, and GB performed experiments. MN, NvdB, and NI developed analytical methods. MN and GB analysed the data. GB supervised the research, constructed the mathematical model, and wrote the manuscript.

Materials and Methods

Culture conditions

Cultures were grown in 250-1000 mL Erlenmeyer flasks filled up to 10% of nominal volume with MOPS minimal medium (42) with 9.5 mM NH_4Cl or $^{15}NH_4Cl$ and 0.2% (w/v) carbon source (acetate, succinate, malate, glycerol, glucose, U-^{13}C-glucose (Cambridge Isotope Laboratories) or glucose supplemented with 0.1% Cas-amino acids). Culture flasks were placed in a Grant Instruments Sub Aqua Pro dual water bath at 37 °C and agitated by stirring with a 12 mm magnetic stir bar (VWR), coupled to a magnetic stir plate (2mag MIXdrive 1 Eco and MIXcontrol 20) set at 1200 rpm. Growth was monitored by optical density measurement at 600

nm using Ultrospec 10 Cell Density Meter (GE Healthcare). Samples for acyl-ACP, lipid analysis and proteomics were collected using cultures without isotopic labelling. Samples for nucleotide phosphate measurements were collected from U-^{15}N-labeled cultures and samples for G3P measurements were collected from U-^{13}C-labeled cultures.

Strains and plasmid pRelA*

All experiments were performed using *Escherichia coli* K-12 strain NCM3722 (CGSC# 12355) and its derivatives. NCM3722 *relA::kan* was constructed by P1 phage transduction using strain CF7974 (MG1655 Δ*lac* (*rph*$^{+}$) *relA255*::*kan)* as a donor. Plasmid pRelA* was created by cloning DNA encoding residues 1-455 from the *E. coli* RelA protein into BglBrick plasmid pBbS2k (43) (SC101* origin of replication, P_{Tet} promoter, kanamycin resistance). The fluorescent protein mVenus was fused by restriction-digestion to the C-terminus of RelA via a glycine-serine linker.

Metabolite sampling

Samples for acyl-ACP, proteomics and lipid analysis were acquired by fast quenching of 1 mL of culture sample into 250 µL of ice-cold 10% trichloroacetic acid. After 10 min incubation at 0°C cells were pelleted by centrifugation and stored at -80°C until analysis. For nucleotide phosphates and polar metabolites analysis, samples were acquired by a modified fast vacuum filtration method (44). 1 mL of culture was collected by vacuum on a pre-wetted 2.5 cm 0.45 µm HV Durapore membrane filter. After rapid collection the filter was immediately placed upside-down in quenching solution. For the measurement of nucleotide phosphates, 1 mL of ice-cold 2 M formic acid with 10 µL internal standards mix was used as a quenching solution, which was subsequently neutralized by 25 µL of 28% ammonium hydroxide. For G3P measurements, 1 mL of 50:30:20 (v/v/v) mixture of methanol, acetonitrile and water with 0.1% formic acid with 10 µL internal standard solution (cooled on dry ice) was used as a quenching solution. After 10 min

incubation cells were washed from the filter, transferred to a tube and stored at -80°C until analysis.

Preparation of internal standards

Isotopically-labeled internal standards (IS) were used to control for sampling and measurement variation. For acyl-ACP and proteomics assays U-^{15}N *E. coli* whole cell extracts were prepared using a MOPS minimal medium culture with $^{15}NH_4Cl$ as the sole nitrogen source. At OD of ~0.5 10% TCA was added 1:4 to the culture to facilitate quenching of metabolism. After 10 min incubation on ice 10 mL single-use IS aliquots were collected by centrifugation and stored at -80°C until the sample preparation. For the phospholipid measurement U-^{13}C lipid extract was prepared using a culture grown in minimal MOPS medium with 0.2% U-^{13}C glucose as the sole carbon source. At OD of ~0.5 10% TCA was added 1:4 to the culture and insoluble cell material was collected by centrifugation after 10 min incubation on ice. Pellets were resuspended in mixture consisting of 75 µL MeOH, 10 µL 15 mM citric acid/ 20 mM dipotassium phosphate buffer and 250 µL of methyl-t-butyl ether per 1 mL of initial culture volume. After vortexing and 10 min sonication phase separation was induced by addition of 70 µL/1mL of 15 mM citric acid/ 20 mM dipotassium phosphate buffer. After further vortexing, sonication and 10 minutes of incubation at room temperature phases were separated by 10 min centrifugation at 4000 rpm at room temperature. Upper phase was collected to a glass vial and stored at -20°C until sample preparation.

Instrumentation

All LC/MS runs were performed using Agilent LCMS consisting of binary pump (G1312B), autosampler (G7167A), temperature-controlled column compartment (G1316A), and triple quadrupole (QQQ) mass spectrometer (G6460C) equipped with a standard ESI source, all operated using MassHunter data acquisition software (version 7.0). Mass spectrometer operated

in dynamic MRM mode using transitions generated *in silico* by a script written in Python using RDkit library using chemical structures of target compound as input. Transitions for targeted proteomics assays were developed using Skyline (45) based on protein sequences from the Uniprot database. Details of transition setting are included in **Supplemental Tables 3-7.**

LC/MS quantification of acyl-ACP intermediates

Acyl-ACP were measured using a published method (18) with minor modifications. Lysis buffer was prepared by suspending appropriate number of frozen U-^{15}N-labeled *E. coli* pellets in 10 mL of 50 mM potassium phosphate buffer, pH 7.2, 6 M urea, 10 mM N-ethyl-maleimide, 5 mM EDTA and 1 mM ascorbic acid. 1 mL of lysis buffer was added to each of TCA-quenched and pelleted cells and proteins were isolated by chloroform/methanol precipitation as described previously. Protein pellets were resuspended in 10 µL of digestion buffer (4% 2-octyl-glucoside in 25 mM potassium phosphate buffer, pH 7.2) and after adding 10 µL of 0.1 mg/mL GluC protease (Promega) incubated overnight at 37°C. After quenching by addition of 5 µL MeOH, samples were centrifuged and 10 µL was injected in LC/MS system. Separation was performed on 2.1 mm x 50 mm 1.7 µm CSH C-18 column (Waters) held at 80°C using a binary gradient: 15% B, 3 minute ramp to 25%, 9 min increase to 95% and 1 minute hold at 95% B before 3 minute re-equilibration at starting conditions (A: 25 mM formic acid, B: 50 mM formic acid) at a flow rate of 0.6 mL/min.

LC/MS quantification of phospholipids

Phospholipids sample preparation procedure is a combination of an MTBE extraction method (46) and an established LC/MS method (47) Pelleted *E. coli* were resuspended in mixture containing 150 µL of MeOH, 250 µL of U-^{13}C *E. coli* extract prepared as described above and 250 µL MTBE. After vigorous vortexing and sonication 125 µL of 15 mM citric acid/ 20 mM dipotassium phosphate buffer was added to homogenized pellets. Following further

vortexing and 10 min incubation at room temperature, liquid phases were separated by centrifugation for 10 min at 20000g. 500 µL the of upper phase was moved to a new tube and dried in a vacuum centrifuge (Labconco). Dried lipid films were resuspended in 10 µL 65:30:5 (v/v/v) isopropanol/acetonitrile/H_2O, supplemented with 10 mM acetylacetone. After resuspension, 5 µL H_2O was added to reduce the organic content of the buffer and 5 µL of resulting mixture was injected into the LC/MS system. Separation was performed on 2.1 mm x 50 mm 1.7 µm CSH C-18 column (Waters) at 60°C with a flow rate of 0.6 mL/min using the following binary gradient: 25% B, ramp to 56%B in 6 min followed by linear increase to 80% B in 6 min, 2 min hold at 100% B and 3 min re-equilibration (A: 0.05% NH4OH in water, B: 0.05% NH_4OH in 80% isopropanol 20% ACN).

LC/MS quantification of nucleotide phosphates

Frozen cell extracts were defrosted by 1-2 minute incubation in a 37°C water bath and sonicated for 10 minutes in water ice slurry. After 10 minute centrifugation at 20000g, samples were loaded on 1 mL/30 mg Oasis Wax cartridge (Waters) preconditioned with 1 mL of MeOH and 1 mL 50 mM ammonium acetate buffer, pH 4.5. After washing with 1 mL ammonium acetate buffer, analytes were eluted with 200 µL of 2.8% ammonium hydroxide in MeOH:ACN:H_2O 50:30:20 (v:v:v). After addition of 10 µL of 5% trehalose and brief vortexing samples were dried down in a vacuum centrifuge (Labconco). Dried trehalose-stabilized extracts were re-dissolved in 20 µL of MeOH:ACN:H_2O 50:30:20 (v:v:v) and moved to an autosampler vial for analysis. Separation was performed on 2.1 mm x 100 mm 3.5 µm iHilic column (HILICON) or SeQuant Zic-cHILIC, 2.1mm x 100 mm, 3µm (Merck) at 0.3 mL/min using the following binary gradient: 100% B, ramp to 85%B in 1.5 min followed by 10 min isocratic hold at 85% B and linear decrease 30% B in 3 minutes with 2 minute hold at 30% B and 8 minute re-equilibration at initial conditions. (A: 3.75 mM ammonium acetate, 1.25 mM acetic acid, 2 mM acetylacetone in MQ, B:

11.25 mM ammonium acetate, 3.75 mM acetic acid, 2 mM acetylacetone in 80% ACN). Injection volume was 2 µL.

LC/MS quantification of G3P

Stored metabolite extracts were dried down in a vacuum centrifuge (Labconco), re-dissolved in 20 µL of MeOH:ACN:H_2O 50:30:20 (v:v:v) and moved to an autosampler vial for analysis. Separation was performed on 2.1 mm x 100 mm 3.5 µm iHilic column (HILICON) at 0.3 mL/min using the following binary gradient: 100% B, ramp to 80% B in 10 min followed by linear decrease to 30% B in 3 min, 2 min hold at 30% B and 8 min re-equilibration. Injection volume was 2 µL.

LC/MS targeted protein quantification

Relative concentrations of enzymes was measured by targeted proteomics using a modified version of the acyl-ACP assay. Lysis buffer was prepared by suspending appropriate number of frozen U-^{15}N-labeled *E. coli* pellets in 10 mL of 50 mM potassium phosphate buffer, pH 7.2 and 6 M urea. 1 mL of lysis buffer was added to each of TCA-quenched and pelleted cells and proteins were isolated by chloroform/methanol precipitation as described previously. Protein pellets were resuspended in 10 µL of digestion buffer (4% 2-octyl-glucoside in 25 mM Tris buffer, pH 8.1 supplemented with 1 mM $CaCl_2$ and 5 mM TCEP). Alkylation of cysteine residues was performed by adding 3 µL of 50 mM iodoacetamide followed by 15 minutes of incubation in darkness. Digestion was performed by adding 10 µL of 0.2 mg/mL Trypsin Gold (Promega) and overnight incubation at 37°C. Samples were centrifuged and 10 µL was injected in LCMS system. Separation was performed on 2.1 mm x 50 mm 1.7 µm CSH C-18 column (Waters) held at 40°C using a binary gradient: 2% B, 20 minute ramp to 25% B, 4 min increase to 40% B, 0.5 ramp to 80% and 1 minute hold at 80% B before 3 minute re-equilibration at starting conditions (A: 25 mL formic acid, B: 50 mM formic acid) at a flow rate of 0.5 mL/min.

Data Analysis

All LC-MS data files were processed in Skyline versions 4.x using target list based on *in silico* generated transition list. Each target compound had matching isotopically-labeled internal standard (IS). Processed data were exported as target compounds and IS peak areas and processed further using a set of Python scripts. Growth rates were obtained from linear fits to log-transformed growth curves. OD-corrected data were obtained by dividing the signal by OD_{600} value interpolated from growth curve at the time of sampling. PE-corrected results were produced by dividing the signal by sum all of signals for all phosphatidyl-ethanolamine species from the same measurement (in case of phospholipids) or matching sample (in case of other assays). In nucleotide phosphate and G3P assay absolute concentrations were estimated based on amounts of internal standards in IS-spike solution assuming RR = 1 implies equimolar amounts of target compound and IS at the moment of quenching. Concentrations of IS in the spike mix are provided in the supplement.

Mathematical modeling

The computational model was constructed and tested using COPASI version 4.24 (48). Full details of the model are described in the **Supplemental Methods**.

References

1. Kamio Y, Nikaido H (1976) Outer Membrane of Salmonella Typhimurium: Accessibility of Phospholipid Head Groups to Phospholipase C and Cyanogen Bromide Activated Dextran in the External Medium. *Biochemistry* 15(12):2561–2570.

2. Funahara Y, Nikaido H (1980) Asymmetric localization of lipopolysaccharides on the outer membrane of Salmonella typhimurium. *J Bacteriol* 141(3):1463–1465.

3. Suzuki H, et al. (1978) Murein-lipoprotein of Escherichia coli: A protein involved in the stabilization of bacterial cell envelope. *MGG Mol Gen Genet* 167(1):1–9.

4. Dowhan W (2013) A retrospective: use of Escherichia coli as a vehicle to study phospholipid synthesis and function. *Biochim Biophys Acta* 1831(3):471–494.

5. Scott M, Gunderson CW, Mateescu EM, Zhang Z, Hwa T (2010) Interdependence of cell growth and gene expression: Origins and consequences. *Science (80-)*. doi:10.1126/science.1192588.

6. Chubukov V, et al. (2013) Transcriptional regulation is insufficient to explain substrate-induced flux changes in Bacillus subtilis. *Mol Syst Biol* 9. doi:Artn 70910.1038/Msb.2013.66.

7. Hackett SR, et al. (2016) Systems-level analysis of mechanisms regulating yeast metabolic flux. *Science (80-)* 354(6311). doi:10.1126/science.aaf2786.

8. Raetz CR, Larson TJ, Dowhan W (1977) Gene cloning for the isolation of enzymes of membrane lipid synthesis: phosphatidylserine synthase overproduction in Escherichia coli. *Proc Natl Acad Sci U S A* 74(4):1412–1416.

9. Ohta A, Waggoner K, Louie K, Dowhan W (1981) Cloning of genes involved in membrane lipid synthesis. Effects of amplification of phosphatidylserine synthase in Escherichia coli. *J Biol Chem*.

10. Ganong BR, Raetz CR (1982) Massive accumulation of phosphatidic acid in conditionally lethal CDP-diglyceride synthetase mutants and cytidine auxotrophs of Escherichia coli. *J Biol Chem* 257(1):389–394.

11. Heacock PN, Dowhan W (1987) Construction of a lethal mutation in the synthesis of the major acidic phospholipids of Escherichia coli. *J Biol Chem* 262(27):13044–13049.

12. Increased synthesis of phosphatidylserine decarboxylase in a strain of Escherichia coli bearing a hybrid plasmid. Altered association of enzyme with the membrane. (1979) *J Biol Chem* 254(3):627–633.

13. Dennis PP, Bremer H (2008) Modulation of Chemical Composition and Other Parameters of the Cell at Different Exponential Growth Rates. *EcoSal Plus* 3(1). doi:10.1128/ecosal.5.2.3.

14. Sud IJ, Schaechter M (1964) Dependence of the content of cell envelopes on the growth rate of Bacillus megaterium. *J Bacteriol* 88(6):1612–1617.

15. Ballesta JPG, Schaechter M (1972) Dependence of the Rate of Synthesis of Phosphatidylethanolamine and Phosphatidylglycerol on the Rate of Growth of Escherichia coli. *J Bacteriol* 110(1):452–453.

16. Schulman H, Kennedy EP (1977) Relation of turnover of membrane phospholipids to synthesis of membrane derived oligosaccharides of Escherichia coli. *J Biol Chem* 252(12):4250–4255.

17. Harris LK, Theriot JA (2016) Relative rates of surface and volume synthesis set bacterial cell size. *Cell* 165(6):1479–1492.

18. Noga MJ, et al. (2016) Mass-Spectrometry-Based Quantification of Protein-Bound Fatty Acid Synthesis Intermediates from Escherichia coli. *J Proteome Res* 15(10):3617–3623.

19. Gerhardt ECM, et al. (2015) The Bacterial signal transduction protein GlnB regulates the committed step in fatty acid biosynthesis by acting as a dissociable regulatory subunit of acetyl-CoA carboxylase. *Mol Microbiol* 95(6):1025–1035.

20. Davis MS, Cronan J (2001) Inhibition of Escherichia coli acetyl coenzyme A carboxylase by acyl-acyl carrier protein. *J Bacteriol*. doi:10.1128/JB.183.4.1499-1503.2001.

21. Wahl A, My L, Dumoulin R, Sturgis JN, Bouveret E (2011) Antagonistic regulation of dgkA and plsB genes of phospholipid synthesis by multiple stress responses in Escherichia coli. *Mol Microbiol* 80(5):1260–1275.

22. Rhodius VA, Suh WC, Nonaka G, West J, Gross CA (2006) Conserved and variable functions of the σEstress response in related genomes. *PLoS Biol*. doi:10.1371/journal.pbio.0040002.

23. Schreiber G, et al. (1991) Overexpression of the relA gene in Escherichia coli. *J Biol Chem* 266(6):3760–3767.

24. Heath RJ, Jackowski S, Rock CO (1994) Guanosine Tetraphosphate Inhibition of Fatty-Acid and Phospholipid-Synthesis in Escherichia coli Is Relieved by Overexpression of Glycerol-3-Phosphate Acyltransferase (PlsB). *J Biol Chem* 269(42):26584–26590.

25. Sorensen PG, et al. (1996) Regulation of UDP-3-O-[R-3-hydroxymyristoyl]-N-acetylglucosamine Deacetylase in Escherichia coli: THE SECOND ENZYMATIC STEP OF LIPID A BIOSYNTHESIS . *J Biol Chem* 271(42):25898–25905.

26. Merlie JP, Pizer LI (1973) Regulation of phospholipid synthesis in Escherichia coli by guanosine tetraphosphate. *J Bacteriol* 116(1):355–366.

27. Nunn WD, Cronan Jr. JE (1976) Regulation of membrane phospholipid synthesis by the relA gene: dependence on ppGpp levels. *Biochemistry* 15(12):2546–2550.

28. Larson TJ, Dowhan W (1976) Ribosomal-Associated Phosphatidylserine Synthetase from Escherichia coli: Purification by Substrate-Specific Elution from Phosphocellulose Using Cytidine 5′-Diphospho-1,2-diacyl-sn-glycerol. *Biochemistry* 15(24):5212–5218.

29. Eichel J, Chang YY, Riesenberg D, Cronan JE (1999) Effect of ppGpp on Escherichia coli cyclopropane fatty acid synthesis is mediated through the RpoS sigma factor (σ(S)). *J Bacteriol* 181(2):572–576.

30. Hofmeyr JHS, Cornish-Bowden A (2000) Regulating the cellular economy of supply and demand. *FEBS Lett*. doi:10.1016/S0014-5793(00)01668-9.

31. Li SJ, Cronan JE (1993) Growth rate regulation of Escherichia coli acetyl coenzyme A carboxylase, which catalyzes the first committed step of lipid biosynthesis. *J Bacteriol* 175(2):332–340.

32. Davidi D, Milo R (2017) Lessons on enzyme kinetics from quantitative proteomics. *Curr Opin Biotechnol* 46:81–89.

33. Ogura T, et al. (1999) Balanced biosynthesis of major membrane components through regulated degradation of the committed enzyme of lipid A biosynthesis by the AAA protease FtsH (HflB) in Escherichia coli. *Mol Microbiol* 31(3):833–844.

34. Emiola A, Andrews SS, Heller C, George J (2016) Crosstalk between the lipopolysaccharide and phospholipid pathways during outer membrane biogenesis in *Escherichia coli*. *Proc Natl Acad Sci* 113(11):3108–3113.

35. Crowfoot PD, Esfahani M, Wakil SJ (1972) Relation Between Protein Synthesis and Phospholipid Synthesis and Turnover in Escherichia coli. *J Bacteriol* 112(3):1408–1415.

36. Lueking DR, Goldfine H (1975) The involvement of guanosine 5-diphosphate-3-diphosphate in the regulation of phospholipid biosynthesis in Escherichia coli. Lack of ppGpp inhibition of acyltransfer from acyl-ACP to sn-glycerol 3-phosphate. *J Biol Chem* 250(13):4911–4917.

37. Nunn WD, Kelly DL, Stumfall MY (1977) Regulation of fatty acid synthesis during the cessation of phospholipid biosynthesis in Escherichia coli. *J Bacteriol* 132(2):526–531.

38. Gully D, Bouveret E (2006) A protein network for phospholipid synthesis uncovered by a variant of the tandem affinity purification method in Escherichia coli. *Proteomics* 6(1):282–293.

39. Carty CE, Ingram LO (1981) Lipid synthesis during the Escherichia coli cell cycle. *J Bacteriol* 145(1):472–478.

40. May KL, Silhavy TJ (2018) The Escherichia coli phospholipase PldA regulates outer membrane homeostasis via lipid signaling. *MBio* 9(2). doi:10.1128/mBio.00379-18.

41. Hermansson M, Hokynar K, Somerharju P (2011) Mechanisms of glycerophospholipid homeostasis in mammalian cells. *Prog Lipid Res* 50(3):240–257.

42. Neidhardt FC, Bloch PL, Smith DF (1974) Culture Medium for Enterobacteria. *J Bacteriol* 119(3):736–747.

43. Lee T, et al. (2011) BglBrick vectors and datasheets: A synthetic biology platform for gene expression. *J Biol Eng* 5(1):12.

44. Link H, Kochanowski K, Sauer U (2013) Systematic identification of allosteric protein-metabolite interactions that control enzyme activity in vivo. *Nat Biotechnol* 31(4):357–361.

45. MacLean B, et al. (2010) Skyline: An open source document editor for creating and analyzing targeted proteomics experiments. *Bioinformatics* 26(7):966–968.

46. Matyash V, Liebisch G, Kurzchalia T V, Shevchenko A, Schwudke D (2008) Lipid extraction by methyl-tert-butyl ether for high-throughput lipidomics. *J Lipid Res* 49(5):1137–1146.

47. Susanto O, et al. (2017) LPP3 mediates self-generation of chemotactic LPA gradients by melanoma cells. *J Cell Sci* 130(20):3455–3466.

48. Hoops S, et al. (2006) COPASI - A COmplex PAthway SImulator. *Bioinformatics* 22(24):3067–3074.

Figures

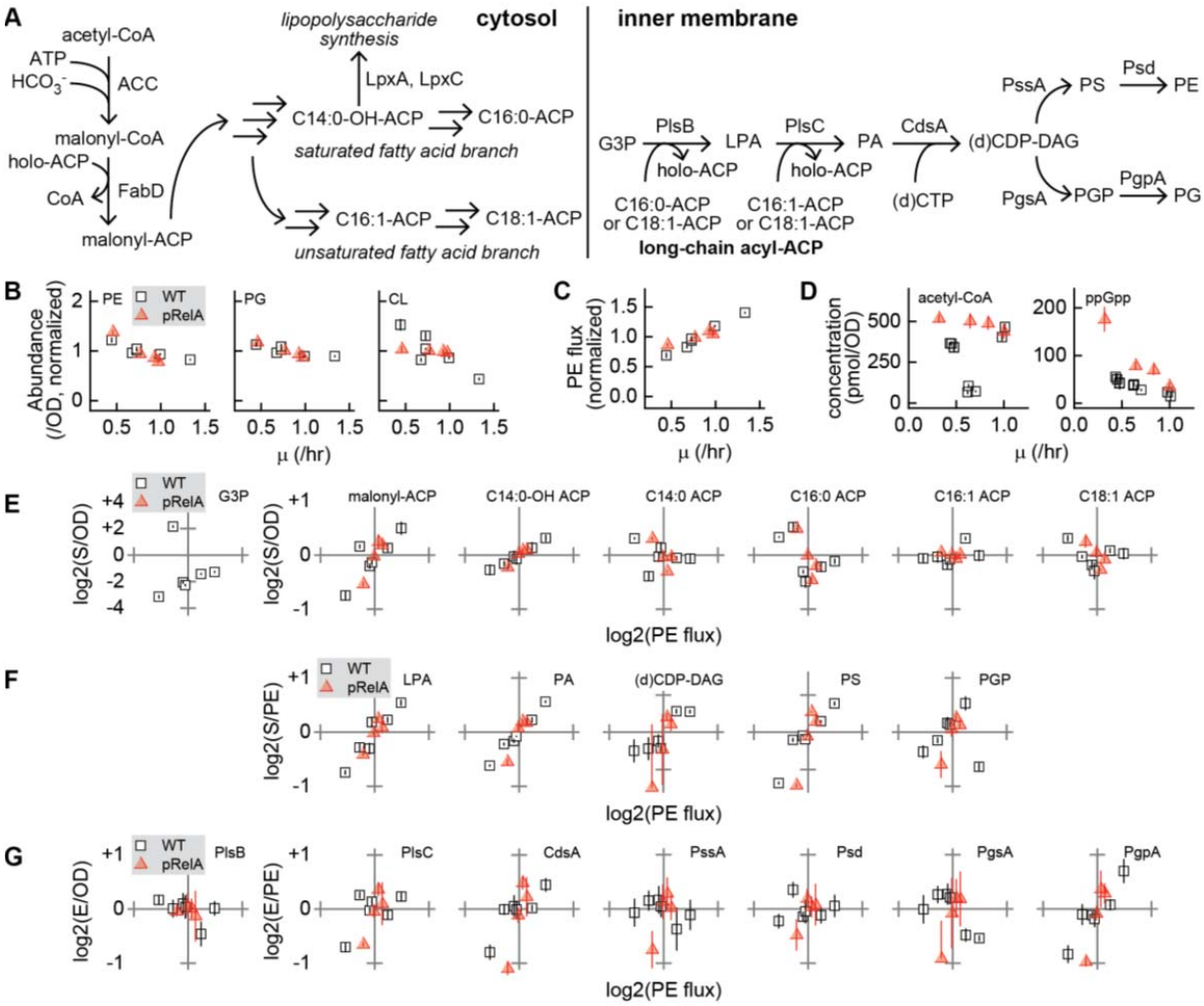

Figure 1. Characterization of the *E. coli* fatty acid and PL synthesis pathways during steady-state growth. **A.** *E. coli* fatty acid and PL synthesis pathways highlighting the metabolites and enzymes discussed in the main text. Fatty acid synthesis is initiated by carboxylation of acetyl-CoA by acetyl-CoA carboxylase complex (ACC) to produce malonyl-CoA, from which the malonyl group is transferred to holo-ACP by FabD. Fatty acids are then elongated by iterated cycles of condensation of acyl-ACP with malonyl-ACP, followed by reduction and dehydration. *sn*-glycerol-3-phosphate (G3P) is acylated by PlsB primarily using long-chain acyl-ACP species C16:0-ACP or C18:1-ACP to yield lysophosphatidic acid (LPA), which is acylated by PlsC using

C16:1-ACP or C18:1-ACP to yield phosphatidic acid (PA). PA is converted by CdsA to (d)CDP-diacylglycerol ((d)CDP-DAG) using either CTP or dCTP. At the branch point in PL synthesis, PgsA combines G3P with (d)CDP-DAG to produce phosphatidylglycerol phosphate (PGP). Dephosphorylation of PGP by PgpA yields PG, which typically comprises 25% of total PL. Two PG molecules may be further converted to CL, which accounts for ~5% of total PL. (d)CDP-DAG is also converted by PssA to phosphatidylserine (PS), which is decarboxylated by Psd to yield PE (70% of total PL). **B, C.** Growth rate (μ)-dependent abundance of total PG, PE, and CL (**B**) and μ-dependence of PE flux (**C**), normalized to average values across conditions for each strain. **D.** Steady-state concentrations of acetyl-CoA and ppGpp. **E, F, G.** Concentrations of G3P and acyl-ACP species **(E)**, PL intermediates **(F)**, and PL synthesis pathway enzymes **(G)** as functions of PL flux. Concentrations of soluble substrates and enzymes with exclusively soluble substrates are calculated using cell volume (proportional to OD). For membrane-bound phospholipid intermediates and for enzymes that react with membrane-bound substrates (all enzymes following PlsB in the PL synthesis pathway) we calculate concentration within the membrane volume, proportional to total PE. *S*/OD, *E*/OD, *S*/PE, and *E*/PE are defined as the concentration of a substrate *S* or enzyme *E* (amount per OD or per PE) relative to its average concentration across all conditions measured in that strain (either wild-type (WT) or pRelA). Values are log(2)-transformed. Error bars represent the standard deviation of measurements from three samples of one culture.

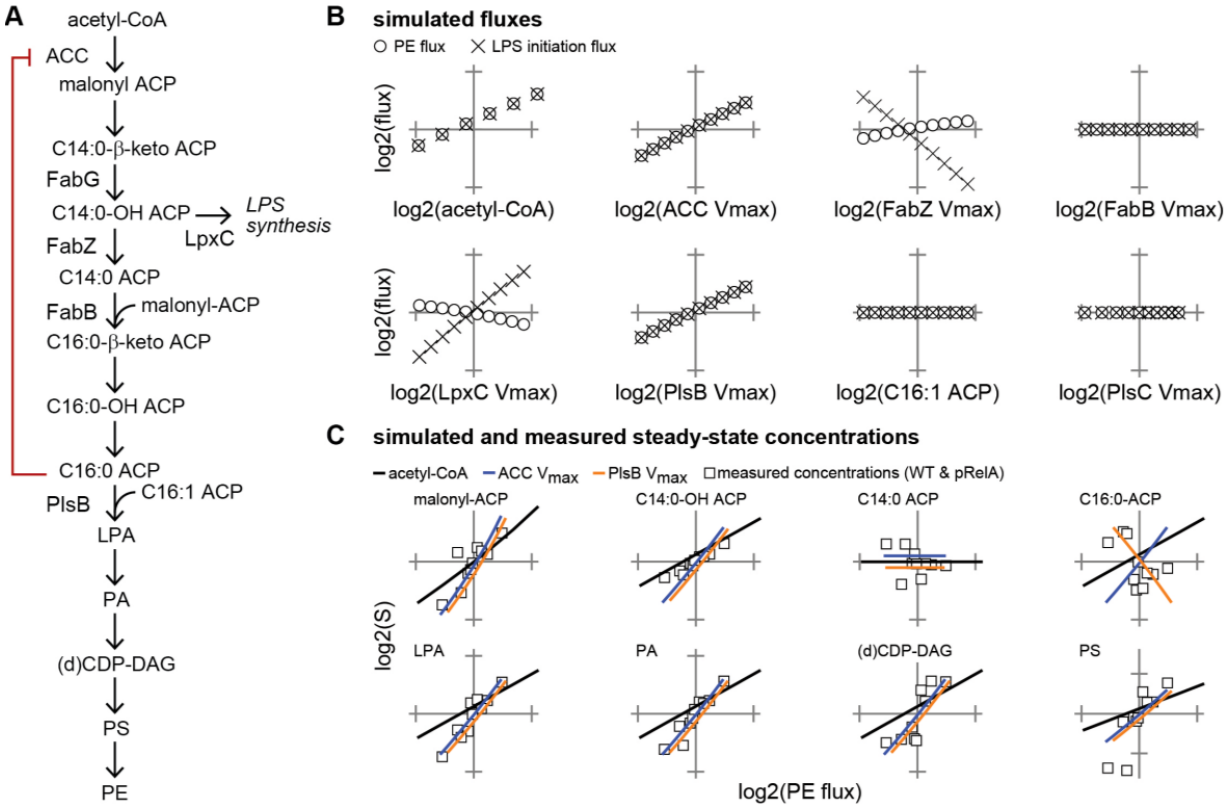

Figure 2. Simulated steady-state fluxes and metabolite concentrations of fatty acid and PL pathways identifies PlsB as site of flux control during steady-state growth. **A.** Reactions simulated in the model. For simplicity, only reactions late in the saturated fatty acid pathway are included, and branching of the PL pathway into PE and PG is not included. Each reaction is modelled as an irreversible one- or two-substrate Michaelis-Menten reaction. ACC activity is competitively inhibited by C16:0-ACP. Reactions catalysed by FabI/FabZ and LpxA/LpxC are considered in the model as single reactions represented by “FabZ” and “LpxC”, respectively. **B.** Response of PE and LPS fluxes to varying V_{max} parameters of pathway enzymes and acetyl-CoA and C16:1-ACP concentrations. 4-fold variations in C14:0-β-keto-ACP synthesis, FabG, CdsA, PssA, and Psd V_{max} did not change PE or LPS flux and are therefore not shown. **C.** Simulated changes in metabolite concentrations in response to variations in PlsB and ACC V_{max} and acetyl-CoA overlaid on experimentally-measured concentrations (data from **Figure 1**). Line plots are offset to prevent overlap. Differential equations and parameters are provided in the

1 **Supplemental Methods**.

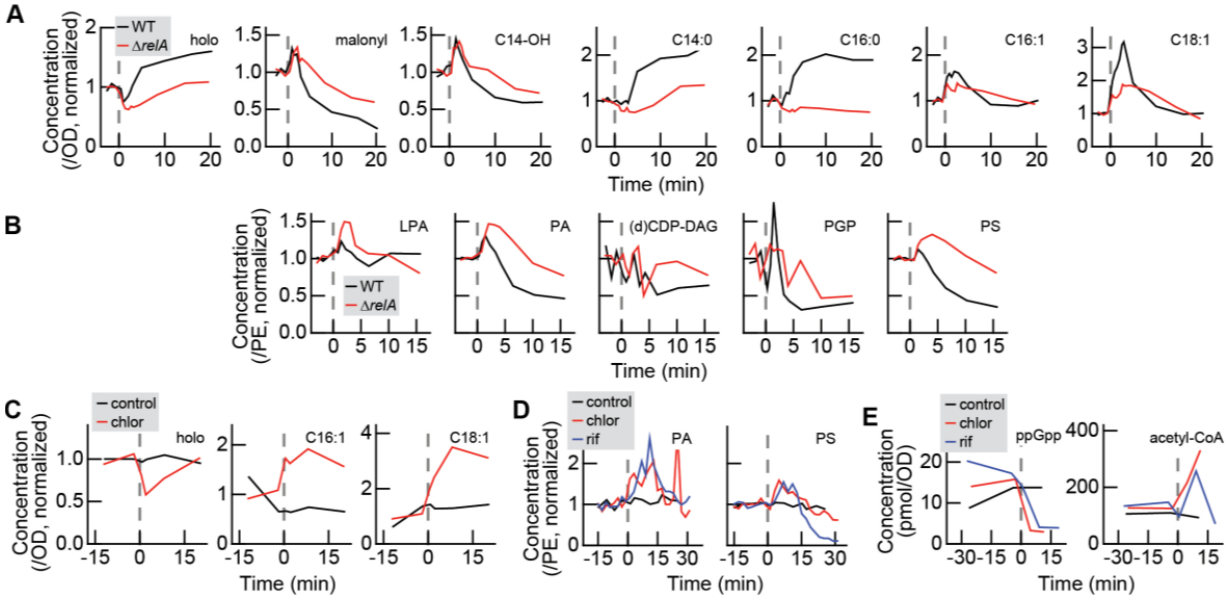

Figure 3. Response of the fatty acid and PL synthesis pathways to translational inhibition. **A, B.** Responses of acyl-ACP **(A)** and PL intermediate pools **(B)** to mupirocin treatment. Mupirocin was added at 0 min (indicated by dashed lines) to glucose cultures of *E. coli* wild-type and Δ*relA*. **C, D.** Addition of translation inhibitor chloramphenicol or the transcription inhibitor rifampicin to glycerol cultures of wild-type *E. coli* (indicated by dashed lines at 0 min) leads to an influx of carbon into the fatty acid pathway as suggested by a decrease in holo-ACP levels and an increase in unsaturated long-chain acyl-ACP species **(C).** The pulse of carbon continues further into the PL synthesis pathway, as indicated by transient increases in total PA and PS **(D).** Trajectories in **A-D** are each obtained from individual cultures. **E.** Chloramphenicol and rifampicin both trigger a rapid decrease in ppGpp and accumulation of ACC and FabH substrate acetyl-CoA. Values depicted in **E** are averages of triplicates from single cultures.

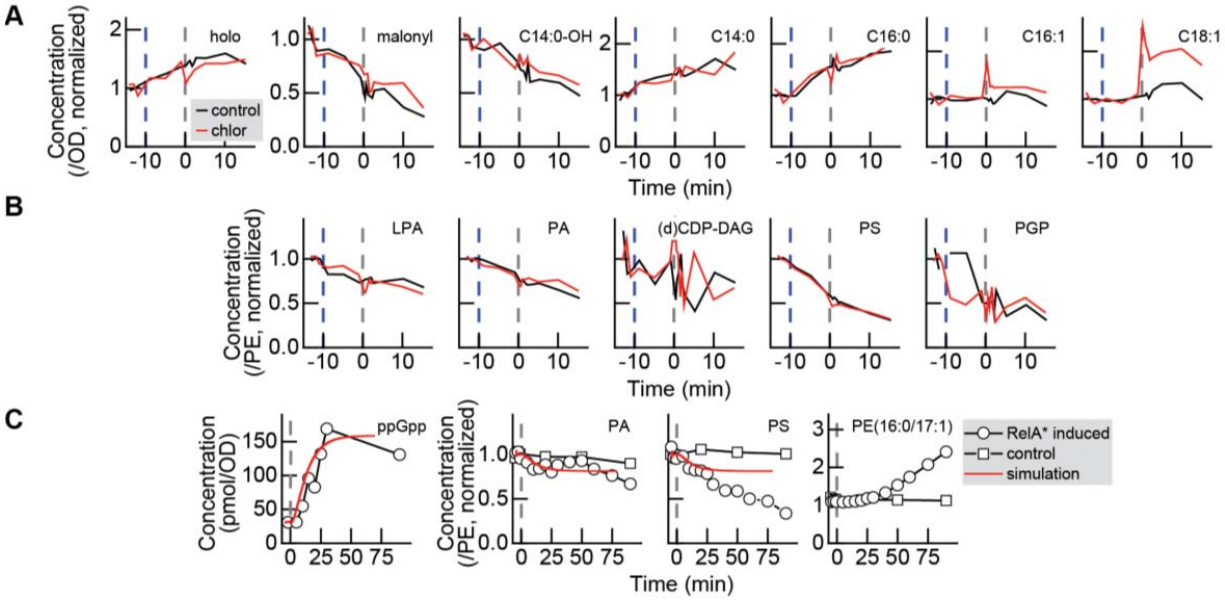

Figure 4. PlsB activity is suppressed by moderate to high concentrations of ppGpp via post-translational inhibition. **A, B.** Response of acyl-ACP **(A)** and PL intermediate pools **(B)** to maximal induction of RelA*. RelA* expression was induced by addition of 40 ng/mL doxycycline at -10 minutes (dashed blue line), followed 10 minutes later by chloramphenicol addition (dashed grey line at 0 min). **C.** Response of PL intermediates and cyclopropyl-PE to mild induction of RelA* expression by addition of 1 ng/mL doxycycline (dashed grey line at 0 min). Superimposed are simulated kinetic data assuming allosteric inhibition of PlsB by ppGpp with an empirical allosteric inhibition constant K_I = 300 pmol/OD. Simulation details are included in the **Supplemental Methods.**

1